

ARTICLE

Chemotherapeutic xCT inhibitors sorafenib and erastin unraveled with the synaptic optogenetic function analysis tool

Marc Dahlmanns¹, Eduard Yakubov^{2,3}, Daishi Chen², Tina Sehm², Manfred Rauh⁴, Nicolai Savaskan^{2,5,6} and Jana Katharina Wrosch^{1,6}

In the search for new potential chemotherapeutics, the compounds' toxicity to healthy cells is an important factor. The brain with its functional units, the neurons, is especially endangered during the radio- and chemotherapeutic treatment of brain tumors. The effect of the potential compounds not only on neuronal survival but also neuronal function needs to be taken into account. Therefore, in this study we aimed to comprehend the biological effects of chemotherapeutic xCT inhibition on healthy neuronal cells with our synaptic optogenetic function analysis tool (SOFA). We combined common approaches, such as investigation of morphological markers, neuronal function and cell metabolism. The glutamate-cystine exchanger xCT (SLC7A11, system X_C⁻) is the main glutamate exporter in malignant brain tumors and as such a relevant drug target for treating deadly glioblastomas (WHO grades III and IV). Recently, two small molecules termed sorafenib (Nexavar) and erastin have been found to efficiently block xCT function. We investigated neuronal morphology, metabolic secretome profiles, synaptic function and cell metabolism of primary hippocampal cultures (containing neurons and glial cells) treated with sorafenib and erastin in clinically relevant concentrations. We found that sorafenib severely damaged neurons already after 24 h of treatment. Noteworthy, also at a lower concentration, where no morphological damage or metabolic disturbance was monitored, sorafenib still interfered with synaptic and metabolic homeostasis. In contrast, erastin-treated neurons displayed mostly inconspicuous morphology and metabolic rates. Key parameters of proper neuronal function, such as synaptic vesicle pool sizes, were however disrupted following erastin application. In conclusion, our data revealed that while sorafenib and erastin effectively inhibited xCT function they also interfered with essential neuronal (synaptic) function. These findings highlight the particular importance of investigating the effects of potential neurooncological and general cancer chemotherapeutics also on healthy neuronal cells and their function as revealed by the SOFA tool.

Cell Death Discovery (2017) 3, 17030; doi:10.1038/cddiscovery.2017.30; published online 19 June 2017

INTRODUCTION

Malignant gliomas (glioblastomas (GBMs; WHO grades III and IV)) are primary brain tumors with lethal prognosis in adults.^{1–3} The median survival time from diagnosis is ~14 months.^{1,3} GBMs are hallmarked by features such as uncontrolled cellular proliferation, diffuse infiltration, and resistance to apoptosis and chemotherapy. The current standard-of-care for GBM patients includes adjuvant temozolomide treatment (brand names Temodal in Europe and Temcad in the USA).⁴ This treatment strategy is currently the best clinical practice, however, conferring still a median survival time of only 14.6 months⁴ compared with 12.2 months for patients receiving only radiotherapy.⁵

Temozolomide, or rather its metabolites, methylate DNA to inhibit tumor proliferation. However, the drug's effects on healthy cells of the patient's body can cause a number of adverse effects resulting from target effects as well as off-target (non-selective) effects. Temozolomide comes along with side effects, such as gastrointestinal irritations, myelosuppression, lymphopenia and opportunistic infections.⁶ This and most importantly the low 5-year survival rate demand the development of new treatment options for glioblastoma. In the hunt for new drugs, researchers

aim to find compounds that are more efficient in cancer cells and more specific to them, so that they spare normal, healthy cells.

Recent evidence has spotlighted the glutamate-cystine exchanger xCT (SLC7A11, system X_C⁻) as a potential drug target in treating glioblastoma.^{7,8} The xCT system represents a key player in glutamate, cystine and glutathione metabolism in most cells.^{2,9} xCT is highly expressed in astrocytes and has also been found in glioblastoma promoting chemotherapeutic resistance.¹⁰ Moreover, xCT levels are causally linked with the malignancy grade of glioblastoma.^{7,11} Apoptosis is a common form of programmed cell death that can be triggered by chemotherapeutic drugs via the intrinsic or extrinsic pathways. Recently, it has been shown that the glutamate cystine exchanger xCT appears to be essential in the process of chemo- and ferroptosis resistance in some cancer cell type.^{12–14} Evasion of cell death and development of redox stability are hallmarks of cancers and promote tumorigenesis as well as chemo-resistance. Since xCT plays a pivotal role in tumor microenvironment interactions, for example, in the induction of peritumoral neuronal cell death and perifocal edema,^{2,11} there is a quest for understanding the effects of inhibiting compounds for this transporter.¹⁵ A deeper understanding of the effects of xCT inhibition on tumor cells might lead to the development of

¹Department of Psychiatry and Psychotherapy, Friedrich-Alexander University of Erlangen-Nuremberg, Erlangen, Germany; ²Translational Neurooncology Laboratory, Department of Neurosurgery, Friedrich-Alexander University of Erlangen-Nuremberg, Erlangen, Germany; ³Paracelsus Medical University, Nuremberg, Germany; ⁴Department of Pediatrics and Adolescent Medicine, Friedrich-Alexander University of Erlangen-Nuremberg, Erlangen, Germany and ⁵BiMECON Ent., Berlin, Germany.

Correspondence: N Savaskan (savaskan@gmx.net or nic.savaskan@gmail.com)

⁶These authors contributed equally to this work.

Received 5 April 2017; accepted 23 April 2017; Edited by A Rufini

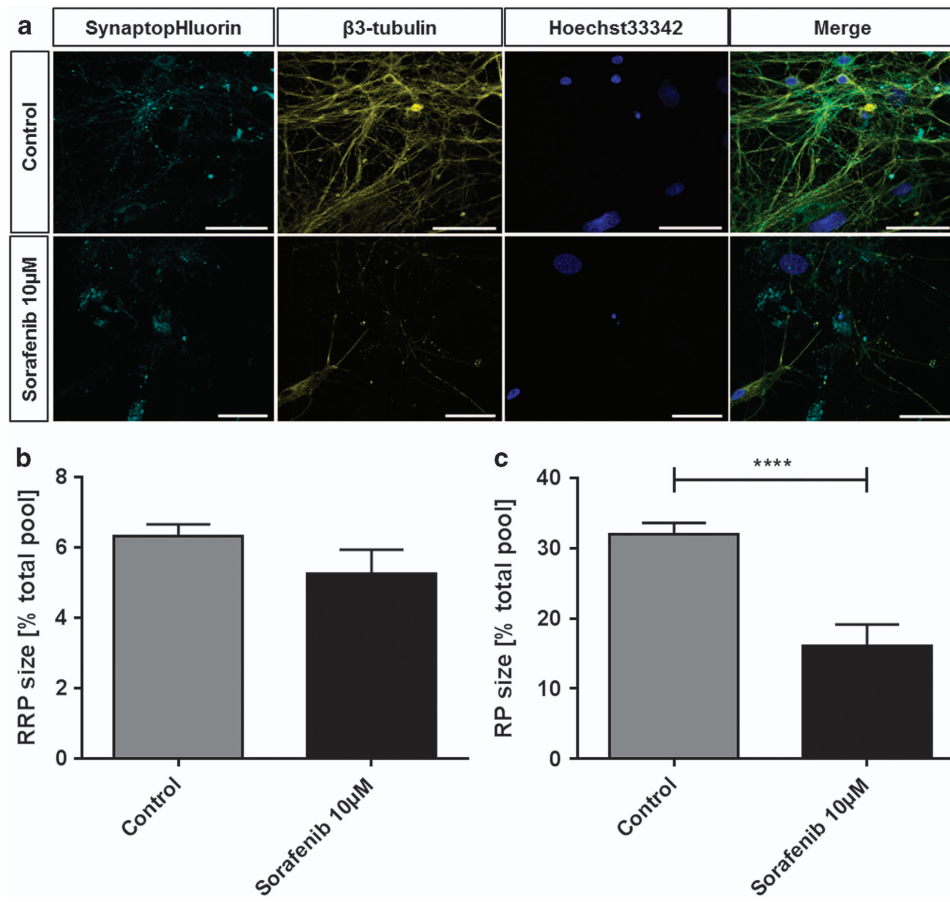


Figure 1. Sorafenib induces morphological alterations and reduces the synaptic vesicle pools in neurons. (a) Representative recordings of neurons treated with 10 μ M sorafenib (lower row) or controls (upper row) for 24 h. The samples were transfected with an EGFP-synaptobrevin2 (synaptopHluorin) construct to visualize vesicles, stained against β 3-tubulin to visualize the neurites and stained with Hoechst33342 that stains the nuclei. The scale bars span 50 μ m. (b) After a 24 h 10 μ M sorafenib treatment (or control), the readily releasable synaptic vesicle pool (RRP) size (released upon electrical stimulation with 40 stimuli at 20 Hz) was measured relative to the total vesicle population (perfusion with 50 mM ammonium chloride) for each synapse. The bar plot shows means with standard errors of the mean. Number of experiments: $n = 32$ for control, $n = 7$ for 10 μ M sorafenib; unpaired two-sided t -test, $P = 0.2013$. (c) After a 24 h 10 μ M sorafenib treatment (or control), the synaptic vesicle recycling pool (RP) size (released upon electrical stimulation with 1200 stimuli at 40 Hz) was measured relative to the total vesicle population (perfusion with 50 mM ammonium chloride) for each synapse. The bar plot shows means with standard errors of the mean. Numbers of experiments: $n = 32$ for control, $n = 7$ for 10 μ M sorafenib; unpaired two-sided t -test, **** $P = 0.0002$.

compounds that break through these tumors' chemo-resistance, and the elucidation of xCT-inhibitor interaction with healthy brain cells might enable us to develop compounds with less adverse, off-target effects.

The xCT inhibitor sorafenib (Nexavar, Bayer Healthcare Pharmaceuticals Inc., Whippany, NJ, USA) is currently approved by EMA and FDA for hepatocellular carcinoma,¹⁶ advanced renal cell carcinoma and thyroid carcinoma.^{17,18} Sorafenib is a multi-kinase inhibitor with various targets inside the cellular signaling cascades.¹⁹ Since a tightly regulated kinase network inside cancer cells is inevitably necessary for signal transduction and tumor growth, treatment with sorafenib impairs cell survival of these tumor cells, for example, in neuroblastoma²⁰ or hepatocellular carcinoma²¹ models. With sorafenib being able to cross the blood-brain barrier it is a prospective substance to treat brain tumors, as well.²² In a phase II clinical trial, sorafenib was already investigated in combination with temozolomide for treatment of relapsed glioblastoma, showing high efficacy.²³ In addition to effectively targeting the tumor cells, a promising chemotherapeutic should also target the tumor specifically. With regard to malignant brain tumors, possible unintended effects of

therapeutic agents on neuronal and astrocyte functions are of particular interest.

In this study, we systematically investigate the effect of chemotherapeutically relevant concentrations of sorafenib on healthy rat hippocampal cells (mainly neurons and astrocytes). To isolate the xCT-inhibition effect of sorafenib, the experiments were conducted in parallel with erastin, a common and well-studied^{8,24-27} model substance for xCT inhibition.

Similar to sorafenib, erastin has been recognized as xCT inhibitor with shown efficacy against tumor cell lines.⁸ Next to impairing amino acids' transport over the membrane, erastin disrupts mitochondrial permeability transition pore (mPTP) and targets the voltage-dependent anion channel 1 (VDAC-1), mechanisms by which erastin could directly interfere with the mitochondrial energy supply of the cells.²⁸⁻³⁰ Metabolically highly active cells such as tumor cells will rapidly be depleted of required substrates and can no longer maintain cell integrity. Recently it was shown that erastin sensitizes glioblastoma cells to temozolomide, an effect that was dependent on xCT inhibition.^{26,31} Although two human studies reported psychotic disorders³² and an impairment of cognitive function³³ after sorafenib treatment, the effects of sorafenib on neurons are sparsely investigated.^{34,35}

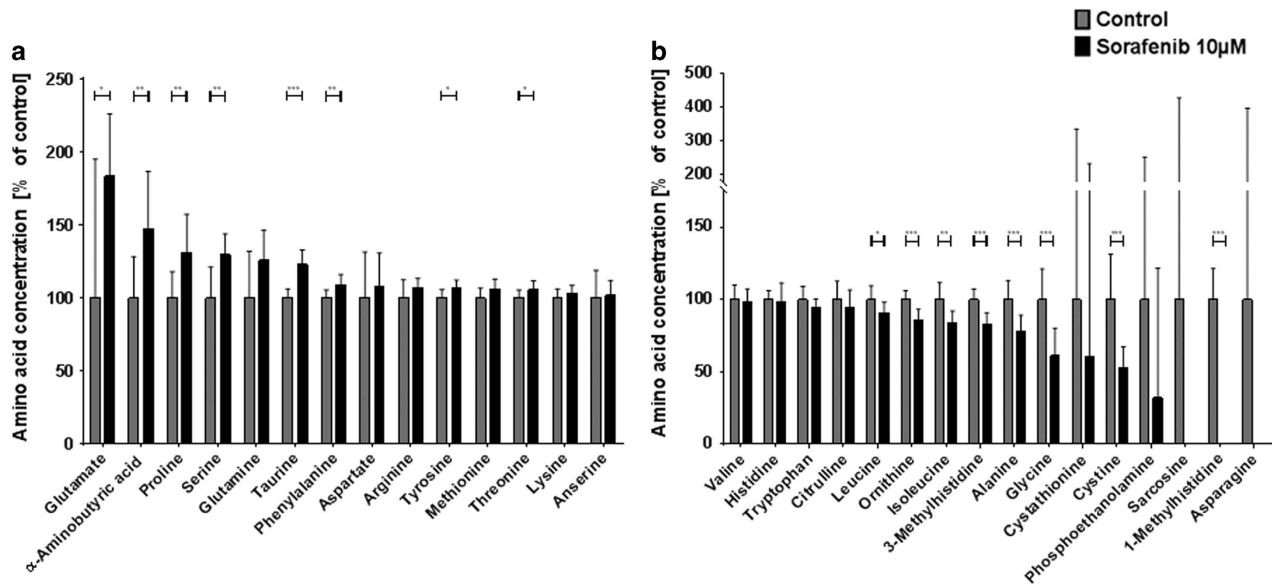


Figure 2. Sorafenib disturbs the extracellular amino acid profile of neurons. Primary hippocampus cultures were incubated with 10 μM sorafenib (or control) for 24 h and their supernatant was collected and analyzed by high-performance liquid chromatography (HPLC). **(a)** Amino acids upregulated in response to 10 μM sorafenib treatment with their concentration relative to the respective controls. Asterisks indicate the level of significance in an unpaired two-sided *t*-test. The bar plot shows means with standard deviations. Numbers of experiments: *n* = 12 for control, *n* = 8 for 10 μM sorafenib. **(b)** Amino acids downregulated in response to 10 μM sorafenib treatment with their concentration relative to the respective controls. Asterisks indicate the level of significance in an unpaired two-sided *t*-test. The bar plot shows means with standard deviations. Numbers of experiments: *n* = 12 for control, *n* = 8 for 10 μM sorafenib. Levels of significance: **P* < 0.05, ***P* < 0.01, ****P* < 0.001. A comprehensive table of all descriptive statistics and the analysis parameters can be found in Table 1.

Also, erastin has, to our knowledge, only been used to induce ferroptosis in immortalized hippocampal cell lines.³⁶ The relevant cytotoxicity of the two substances has not been investigated up to now.

Noteworthy, many previous studies ensure neurons safety by evaluating single morphological markers.^{37–40} In some studies the amino-acid profile of treated cells has been quantified.^{41,42} In this report, we applied the synaptic optogenetic function analysis (SOFA) tool to unravel sub-morphological changes of neurons. With the SOFA tool at hand, we investigated cell survival and synaptic functional parameters in neurons treated with chemotherapeutics. We found that only with a combination of multiple viability assays and functional tools one can gain a comprehensive picture of a compound's neurotoxic profile, especially if the effects are subtle. Key to neuronal function is the ability of neurotransmission, that is, the exocytosis of synaptic neurotransmitters, stored in synaptic vesicles, into the neural cleft where they bind to a postsynaptic receptor.⁴³ The total pool of a neuron's synaptic vesicles is well organized into different functional groups: the readily releasable pool, the recycling pool and the reserve pool.⁴⁴ Neurons' vesicle pool sizes are complex and highly regulated systems. Its dynamics are part of presynaptic plasticity and an unbalanced homeostasis is involved in different psychiatric and neurological disorders.^{45–48} Major depressive disorder—one of the common adverse effects of glioblastoma treatment⁴⁹—has been related to a vesicle pool size pathology.⁵⁰ Quantifying the vesicle pool sizes of neurons treated with sorafenib and erastin therefore is a valuable addition to the common approaches on drug safety.

Key to the SOFA tool is a widespread approach for measuring synaptic vesicle pool sizes by use of pHluorin constructs.⁵¹ In brief, pHluorins are vesicular proteins, labeled by a pH-dependent fluorescence component. While fluorescence is quenched by the low pH inside the synaptic vesicle, upon a vesicle-membrane fusion event the molecules are exposed to the neutral pH of the synaptic cleft, emit fluorescence and can be recorded. With different external stimulation manoeuvres, the neurons are

triggered to release synaptic vesicles of specific vesicle pools (e.g. readily releasable pool) whose size can then be quantified as the number of vesicles exocytosed upon stimulation.

Next to shedding light onto the effects of xCT inhibition on synaptic vesicle populations, our data highlight the importance of taking possible neuronal damage into account when designing new treatments for brain cancer. Approaching the concept of unintended and cytotoxic effects with the SOFA tool, we gain a comprehensive picture and can set morphological observations into context with metabolic and functional parameters.

RESULTS

Our first interest was to assess sorafenib's effects on neuronal cell morphology, synaptic vesicle pool sizes, amino-acid secretome profiles and metabolic rates.

At the concentration of 10 μM, that proved efficient in targeting tumor cells in Dixon *et al.*⁸, we found that neurons also suffered from sorafenib treatment. Figure 1a shows exemplary recordings of cultures treated with 10 μM for 24 h. Compared to the colocalized vesicles and neurites seen in the control group, aggregates of synaptic vesicles are forming instead. The usual synaptic puncta staining pattern of the spH-transfected cells is lost. Also the extent to which the cytoskeleton is affected by the treatment with 10 μM sorafenib is clearly visible. These features witness to a damage of the structure and morphology of the neurons in response to 10 μM sorafenib treatment. With regard to synaptic function, the effect becomes even more visible: while basic synaptic architecture can still be maintained (readily releasable pool: control: 6.325 ± 0.348%, *n* = 32, sorafenib: 5.273 ± 0.348%, *n* = 7), the recycling pool is reduced from 31.98 ± 1.642% (*n* = 32) to only 16.04 ± 3.11% (*n* = 7) in the treated neurons (Figure 1b and c). In addition to this strong interference with synaptic vesicle recycling, electrical excitability, that is, the ability to induce synaptic vesicular release, was unusually weak in the treated group (data not shown), which also explains this experimental group's lower sample size.

Table 1. Amino-acid profiles of mixed neuronal cultures after treatment with xCT-inhibitors sorafenib and erastin

Amino acid	Control n = 12	Sorafenib 10 μ M n = 8	Sorafenib 5 μ M n = 10	Erastin 10 μ M n = 12
Glutamate	100.00 \pm 27.40 [~]	183.49 \pm 14.05, P = 0.03218[^]	290.48 \pm 58.01, P = 0.00518[^]	390.86 \pm 43.45, P = 0.00002[^]
α -Aminobutyric acid	100.00 \pm 8.19 [~]	147.11 \pm 13.03, P = 0.00593[^]	30.04 \pm 7.08, P < 0.00001[^]	103.69 \pm 3.75, P = 0.68846 [~]
Proline	100.00 \pm 5.19 [~]	130.82 \pm 8.73, P = 0.00590[^]	159.98 \pm 7.96, P < 0.00001[^]	103.59 \pm 3.78, P = 0.58784 [~]
Serine	100.00 \pm 6.09 [~]	129.33 \pm 4.79, P = 0.00306[^]	142.10 \pm 4.03, P = 0.00002[^]	98.35 \pm 4.46, P = 0.83189 [~]
Glutamine	100.00 \pm 9.20 [~]	125.72 \pm 6.85, P = 0.05996 [^]	234.19 \pm 5.44, P < 0.00001[^]	93.63 \pm 8.15, P = 0.61632 [~]
Taurine	100.00 \pm 1.78 [~]	122.65 \pm 3.39, P = 0.00001[^]	117.07 \pm 3.45, P = 0.00016[~]	105.78 \pm 2.85, P = 0.10965 [~]
Phenylalanine	100.00 \pm 1.59 [~]	109.13 \pm 2.25, P = 0.00392[~]	105.10 \pm 2.72, P = 0.10772 [~]	102.58 \pm 2.07, P = 0.34757 [~]
Aspartate	100.00 \pm 9.08 [~]	108.21 \pm 7.46, P = 0.53348 [~]	119.68 \pm 9.76, P = 0.15611 [~]	114.01 \pm 6.37, P = 0.22609 [~]
Arginine	100.00 \pm 3.54 [~]	106.80 \pm 2.15, P = 0.16980 [~]	65.34 \pm 1.76, P < 0.00001[^]	101.91 \pm 4.08, P = 0.73408 [~]
Tyrosine	100.00 \pm 1.65 [~]	106.33 \pm 1.95, P = 0.02756[~]	101.25 \pm 2.34, P = 0.65815 [~]	101.57 \pm 2.02, P = 0.56312 [~]
Methionine	100.00 \pm 1.91 [~]	106.28 \pm 2.18, P = 0.05184 [~]	95.15 \pm 2.32, P = 0.11844 [~]	102.35 \pm 2.83, P = 0.51026 [~]
Threonine	100.00 \pm 1.57 [~]	105.80 \pm 1.95, P = 0.03645[~]	103.34 \pm 2.57, P = 0.26301 [~]	102.72 \pm 2.04, P = 0.31588 [~]
Lysine	100.00 \pm 1.74 [~]	102.66 \pm 1.98, P = 0.34607 [~]	98.53 \pm 2.34, P = 0.61395 [~]	103.83 \pm 2.17, P = 0.19347 [~]
Asparagine	100.00 \pm 5.47 [~]	101.53 \pm 3.49, P = 0.83874 [~]	79.08 \pm 2.62, P = 0.00416[~]	96.87 \pm 4.95, P = 0.68151 [~]
Valine	100.00 \pm 2.90 [~]	98.67 \pm 2.88, P = 0.76430 [~]	66.59 \pm 1.42, P < 0.00001[^]	105.53 \pm 2.75, P = 0.18892 [~]
Histidine	100.00 \pm 1.77 [~]	98.23 \pm 4.34, P = 0.68729 [~]	97.55 \pm 2.24, P = 0.39382 [~]	101.44 \pm 2.15, P = 0.61966 [~]
Tryptophan	100.00 \pm 2.57 [~]	94.24 \pm 2.03, P = 0.12967 [~]	83.57 \pm 3.30, P = 0.00073[~]	98.34 \pm 2.34, P = 0.64500 [~]
Citrulline	100.00 \pm 3.63 [~]	94.24 \pm 4.05, P = 0.32358 [~]	99.64 \pm 2.45, P = 0.93849 [~]	100.26 \pm 2.99, P = 0.95762 [~]
Leucine	100.00 \pm 2.76 [~]	90.58 \pm 2.53, P = 0.03185[~]	50.33 \pm 1.43, P < 0.00001[^]	102.62 \pm 3.19, P = 0.55057 [~]
Ornithine	100.00 \pm 1.76 [~]	85.73 \pm 2.48, P = 0.00018[~]	80.98 \pm 1.72, P < 0.00001[~]	101.70 \pm 2.32, P = 0.57471 [~]
Isoleucine	100.00 \pm 3.39 [~]	83.65 \pm 2.82, P = 0.00335[~]	42.37 \pm 1.35, P < 0.00001[^]	103.74 \pm 3.72, P = 0.47555 [~]
1-Methylhistidine	100.00 \pm 2.10 [~]	82.76 \pm 2.71, P = 0.00010[~]	76.14 \pm 6.14, P = 0.00078[~]	96.58 \pm 2.55, P = 0.32288 [~]
Alanine	100.00 \pm 3.78 [~]	77.66 \pm 3.79, P = 0.00100[~]	47.56 \pm 2.32, P < 0.00001[^]	102.62 \pm 2.07, P = 0.55292 [~]
Glycine	100.00 \pm 6.09 [~]	61.26 \pm 6.24, P = 0.00055[~]	7.76 \pm 0.61, P < 0.00001[^]	99.95 \pm 5.61, P = 0.99552 [~]
Cystathionine	100.00 \pm 67.67 [~]	60.32 \pm 56.42, P = 0.68645 [~]	1382.22 \pm 86.94, P < 0.00001[^]	0.00 \pm 0.00, P = 0.15367 [~]
Cystine	100.00 \pm 9.07 [~]	52.73 \pm 4.79, P = 0.00092[~]	18.61 \pm 0.79, P < 0.00001[^]	93.20 \pm 10.72, P = 0.64189 [~]
Phosphoethanolamine	100.00 \pm 43.56 [~]	31.76 \pm 29.71, P = 0.26730 [~]	61.69 \pm 41.13, P = 0.53549 [~]	134.64 \pm 49.00, P = 0.61143 [^]
Sarcosine	100.00 \pm 94.84 [~]	0.00 \pm 0.00, P = 0.40485 [~]	0.00 \pm 0.00, P = 0.34924 [~]	0.08 \pm 0.08, P = 0.30354 [~]
1-Methylhistidine	100.00 \pm 6.14 [~]	0.00 \pm 0.00, P < 0.00001[^]	0.00 \pm 0.00, P < 0.00001[^]	99.10 \pm 5.38, P = 0.91462 [~]
Anserine	100.00 \pm 85.61 [~]	0.00 \pm 0.00, P = 0.35714 [~]	0.00 \pm 0.00, P = 0.30092 [~]	0.00 \pm 0.00, P = 0.25525 [~]

The levels of amino acids and metabolites in extra cellular fluid are changed after treatment with different concentrations of sorafenib and erastin. Presented values are given as percent of untreated controls. The values are shown as mean \pm standard error of the mean (SEM) and with P-values for two-sided t-tests. Upregulated amino acids are marked with [^], medium regulated amino acids (80%–120% of controls) are marked with [~], downregulated amino acids are unmarked; alterations which are statistically significant are highlighted in bold font.

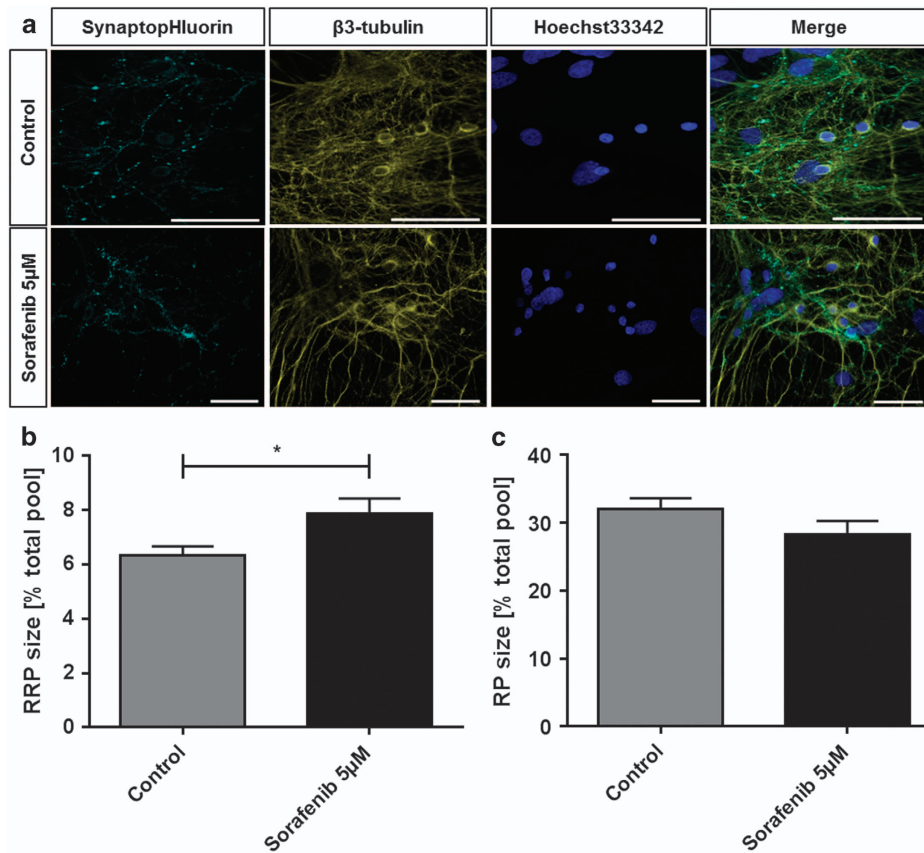


Figure 3. Low-dose sorafenib treatment does not affect neuronal morphology but impairs neuronal function by increasing the synaptic readily releasable pool. **(a)** Exemplary recordings of cells treated with 5 μM sorafenib (lower row) or controls (upper row) for 24 h. The samples were transfected with EGFP-synaptobrevin2 (synaptopHluorin) to visualize vesicles, stained against β3-tubulin to visualize the neurites and stained with Hoechst33342 that stains the nuclei. The scale bars span 50 μm. **(b)** After a 24 h 5 μM sorafenib treatment (or control), the readily releasable synaptic vesicle pool (RRP) size (released upon electrical stimulation with 40 stimuli at 20 Hz) was measured relative to the total vesicle population (perfusion with 50 mM ammonium chloride) for each synapse. The bar plot shows means with standard errors of the mean. Number of experiments: $n = 32$ for control, $n = 21$ for 5 μM sorafenib; unpaired two-sided t -test, $*P = 0.018$. **(c)** After a 24 h 5 μM sorafenib treatment (or control), the synaptic vesicle recycling pool (RP) size (released upon electrical stimulation with 1200 stimuli at 40 Hz) was measured relative to the total vesicle population (perfusion with 50 mM ammonium chloride) for each synapse. The bar plot shows means with standard errors of the mean. Number of experiments: $n = 32$ for control, $n = 21$ for 5 μM sorafenib; unpaired two-sided t -test, $P = 0.161$.

In agreement with the morphologically and functionally apparent damage, the amino-acid profile of cultures treated with 10 μM sorafenib was massively disturbed (Figure 2). We observed an almost doubled concentration of glutamate (183.49% of control $\pm 14.05\%$) and elevated concentrations of the amino acids proline, serine, glutamine, taurine, phenylalanine, aspartate, arginine, tyrosine, methionine and threonine (Figure 2a). A comprehensive list of amino-acid concentrations of all experimental groups and the corresponding statistical analysis are shown in Table 1. Amino-acid concentrations comparable to controls were found for lysine, asparagine, valine, histidine, tryptophan and citrulline, whereas concentrations of leucine, ornithine, isoleucine, 3-methylhistidine, alanine, glycine, cythathionine, cysteine, sarcosine and 1-methylhistidine were found to be lower than in controls (Figure 2b).

Altogether, treatment with 10 μM sorafenib for 24 h lead to enormous morphological and functional alterations, as well as to a disturbed amino-acid profile of the cultures. The damages were so strong that they became apparent in each of our viability assays.

In contrast to these devastating effects of a 10 μM sorafenib treatment, our experiments show that treatment with only 5 μM sorafenib—a concentration that is still efficient in reducing tumor cell growth⁵²—did not affect the cell morphology (Figure 3a). Synapses and neurites align, and neither the pattern of vesicle

staining nor the cytoskeleton or the cell nuclei is changed in their appearance compared to controls.

Despite this seemingly intact morphology of the 5 μM sorafenib-treated cultures, the extended analysis of functional and metabolic parameters still showed severe alterations. The general synaptic vesicle recycling cycle is not disturbed and with that the vesicular recycling pool is unaffected (sorafenib: $28.32 \pm 1.973\%$, $n = 21$; control: $31.98 \pm 1.642\%$, $n = 32$) (Figure 3b). The readily releasable pool (Figure 3c) on the other hand significantly grows from $6.325 \pm 0.3475\%$ ($n = 32$) to $7.860 \pm 0.057\%$ ($n = 21$) in the treated cells—an effect also found in neurons treated with tetrodotoxin.⁵³ Such an increase in readily releasable pool size is accompanied by an increased number of docked vesicles and such a facilitated neurotransmitter release⁵³ constitutes a serious intrusion of neuronal function. As it can be expected from the disturbed synaptic homeostasis, the amino-acid profile of cultures treated with 5 μM sorafenib is also diversely affected by the treatment (Figure 4a and b). Similar to the cultures treated with 10 μM, we find an almost three-fold rise of extracellular glutamate levels in the treated cultures compared to controls (290.48% of control $\pm 55.03\%$). The further amino-acid profile also shows the same up- and downregulation as the 10 μM sorafenib-treated cultures. The only exception is the cystathionine, which is massively increased only in the 5 μM sorafenib-treated

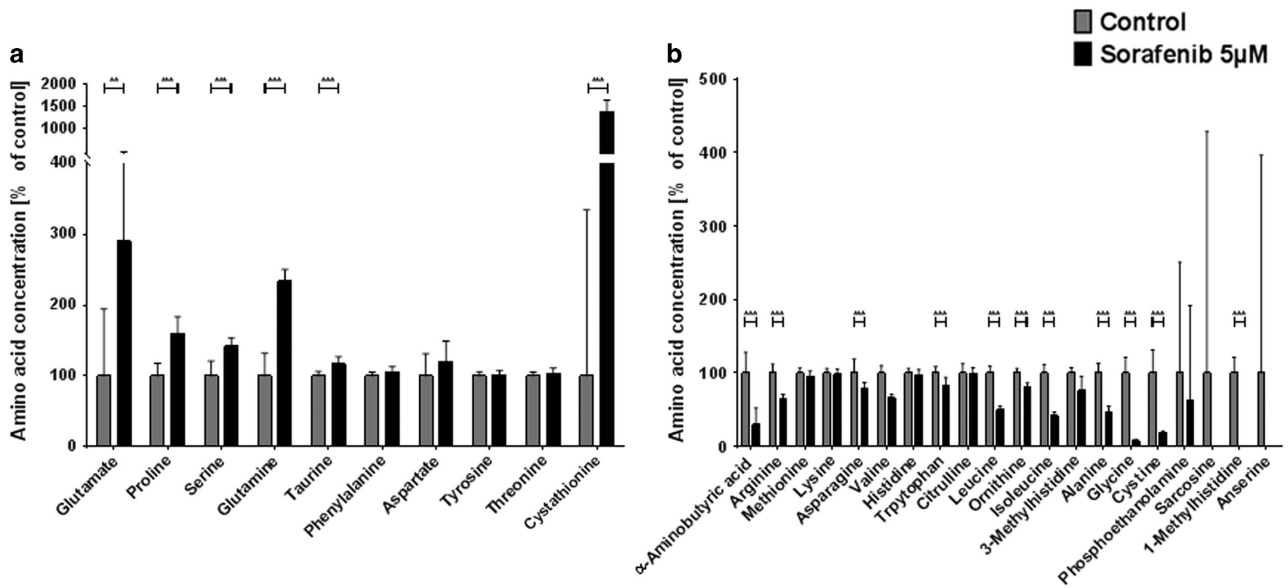


Figure 4. Low-dose sorafenib treatment disturbs the extracellular amino-acid profile of hippocampal cultures. Primary hippocampus cultures were incubated with 5 μM sorafenib (or control) for 24 h and their supernatant was collected and analyzed by high-performance liquid chromatography (HPLC). **(a)** Amino acids upregulated in response to 5 μM sorafenib treatment with their concentration relative to the respective controls. Asterisks indicate the level of significance in an unpaired two-sided *t*-test. The bar plot shows means with standard deviations. Number of experiments: *n* = 12 for control, *n* = 10 for 5 μM sorafenib. **(b)** Amino acids downregulated in response to 5 μM sorafenib treatment with their concentration relative to the respective controls. Asterisks indicate the level of significance in an unpaired two-sided *t*-test. The bar plot shows means with standard deviations. Number of experiments: *n* = 12 for control, *n* = 10 for 5 μM sorafenib. Levels of significance: ***P* < 0.01, ****P* < 0.001. A comprehensive table of all descriptive statistics and the analysis parameters can be found in Table 1.

cultures (10 μM : 60.32 \pm 56.42%; 5 μM : 1382.22 \pm 86.94%) and arginine, which is slightly upregulated after a 10 μM sorafenib treatment, but downregulated after a 5 μM sorafenib treatment (10 μM : 106.80 \pm 1.95%; 5 μM : 65.34 \pm 1.76%).

Although the lower concentration of 5 μM sorafenib—in contrast to the 10 μM concentration—did not suggest any damage in the morphological examination, the investigation of functional parameters and the amino-acid profile reveals an interference of the treatment with the sensitively regulated homeostasis of neuronal cultures and their function. This underlines the importance of an extension of neurotoxicity studies to also include these parameters.

With the previous results, it becomes clear that a treatment of glioblastoma cells *in situ*—surrounded by neurons—could affect proper neuronal function. As sorafenib binds to many different targets on the different cell types, we tried to isolate the effect mediated through the xCT-blockage pathway by comparing these outcomes to those obtained from the experiments with erastin, a different xCT inhibitor.

Despite the known efficacy of erastin on tumor cell lines,⁸ there was no damage visible in the morphological examination of the treated neuronal cultures. The overlay of neurites and vesicles that we observed in untreated controls is not changed after 24 h of 10 μM erastin treatment (Figure 5a). Neither are the cytoskeletons or the cells' nuclei deformed or damaged.

Erastin, next to xCT inhibition, also induces VDAC-1 opening, which upregulates cytosolic calcium concentration.²⁹ The delicate calcium-dependent regulation of synaptic vesicle recycling⁴⁴ responds to the erastin treatment with a readily releasable pool reduced by over one-third compared to controls (control: 6.325% of total pool \pm 0.348%, *n* = 32; 10 μM erastin: 4.138 \pm 0.318%, *n* = 19) (Figure 5b). The overall size of the vesicular recycling pool is not altered in the erastin-treated cultures (control: 31.98 \pm 1.642%, *n* = 32; 10 μM erastin: 30.35 \pm 1.609%, *n* = 19) (Figure 5c). Similar to the selective modulation of presynaptic release probability (readily releasable pool^{54,55}), the analysis of extracellular fluid brought out the same strong increase in glutamate levels (390.86% of control \pm 43.45%) as the xCT

inhibition with sorafenib, but brought out otherwise unchanged amino-acid concentrations (Figure 6a and b).

After revealing the effects of sorafenib and erastin treatment on the extracellular amino-acid regulation, we turned to intracellular metabolism and investigated metabolic rates under the influence of both substances (and controls) using a MTT assay (Figure 7).

We found that despite the deteriorated morphology, cultures treated with 10 μM sorafenib metabolized MTT with the highest rate of all tested groups (113.6% of control \pm 12.5%, *P* < 0.0001). The lower concentration of 5 μM sorafenib had no effect on the cells' metabolic rate compared to controls (96.7 \pm 2.9%, *P* = 0.2320). In contrast to the even enhancing effect of sorafenib, erastin dose-dependently lowered the metabolic rate of the treated cells. Treatment with 5 μM erastin slowed MTT metabolism to only 92.6 \pm 2.6% of the controls (*P* = 0.0067) and treatment with 10 μM erastin yielded a lowered rate of 87.7 \pm 2.7% of controls (*P* < 0.0001).

DISCUSSION

Although sorafenib and erastin are xCT inhibitors, we surprisingly found that treatment with both substances increased the extracellular concentration of glutamate. In view of the importance of glutamate as a neurotransmitter and the complexity of its regulatory network,⁵⁶ it seems clear that inhibition of the antiporter xCT system does not inevitably lead to a reduced extracellular glutamate concentration, at least when there are several different cell types in one culture, for example, astrocytes, neurons and microglia. Although further research is needed to determine what is the main origin of these increased glutamate levels, we hypothesize that inhibiting one part of the system regulating glutamate leads to cell stress and subsequently increases demand for cystine for glutathione generation. These imbalances in the glutathione pool are counteracted by other parts of this system, ultimately increasing the extracellular glutamate concentration.

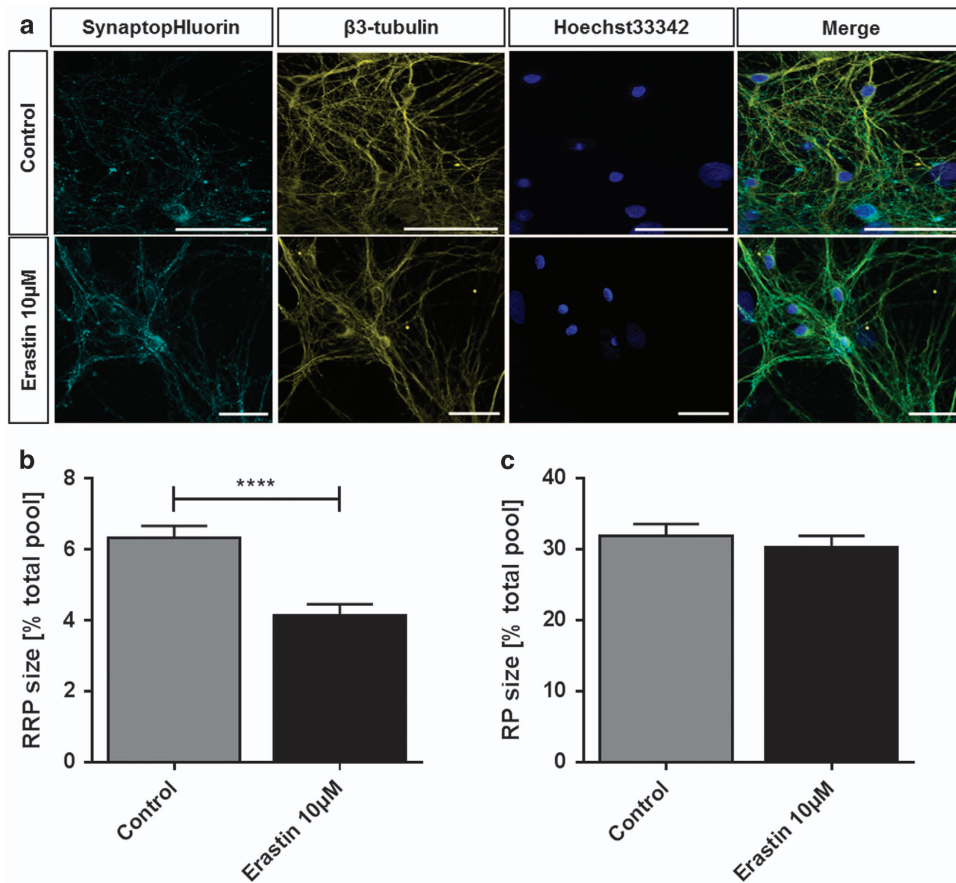


Figure 5. Erastin reduces readily releasable pool size but does not affect recycling pool size or the neuroskeletal architecture. **(a)** Representative recordings of cells treated with 10 μ M erastin (lower row) or controls (upper row) for 24 h. The samples were transfected with EGFP-synaptobrevin2 (synaptopHluorin) to visualize vesicles, stained against β 3-tubulin to visualize the neurites and stained with Hoechst33342 that stains the nuclei. The scale bars span 50 μ m. **(b)** After a 24 h 10 μ M erastin treatment (or control), the readily releasable synaptic vesicle pool (RRP) size (released upon electrical stimulation with 40 stimuli at 20 Hz) was measured relative to the total vesicle population (perfusion with 50 mM ammonium chloride) for each synapse. The bar plot shows means with standard errors of the mean. Number of experiments: $n = 32$ for control, $n = 19$ for 10 μ M erastin; unpaired two-sided t -test, **** $P < 0.0001$. **(c)** After a 24 h 10 μ M erastin treatment (or control), the synaptic vesicle recycling pool (RP) size (released upon electrical stimulation with 1200 stimuli at 40 Hz) was measured relative to the total vesicle population (perfusion with 50 mM ammonium chloride) for each synapse. The bar plot shows means with standard errors of the mean. Number of experiments: $n = 32$ for control, $n = 19$ for 10 μ M erastin; unpaired two-sided t -test, $P = 0.512$.

Our data further show that neither sorafenib nor erastin leaves the mixed hippocampal cells unaffected. The 10 μ M sorafenib treatment massively disturbed neuronal morphology and function, and although MTT metabolism appeared healthy, even enhanced, the amino-acid homeostasis collapsed as it does, for example, also in ischemia.⁵⁷

The lower concentrated 5 μ M sorafenib treatment did not affect neurons as severely. Although still showing an imbalanced amino-acid profile, both the synaptic vesicle recycling pool and cell morphology were preserved. The presynaptic availability of readily releasable vesicles, however, was modified at the lower concentration of 5 μ M sorafenib. The interference with the sensitive regulation of synaptic vesicles is thought to be the underlying cause of many psychiatric disorders⁴⁵ and has been studied in the context of a wide range of neurotoxins.^{53,54}

The reference experiments with erastin showed that even though MTT metabolism is decreased in the erastin-treated cultures, the effects of the substance on cell morphology, synaptic vesicle recycling and the interference with vesicle docking (RRP) are comparable to sorafenib. Yet, erastin did not affect the cultures' extracellular amino-acid profile, which suggests that this part of sorafenib's effects might be due to off-target effects.

These results prove that the sole examination of morphological parameters—as it is common in when evaluating new chemotherapeutic agents^{37–39,58}—might be misleading in the context of neurons.

Morphological parameters are severely affected by a 10 μ M sorafenib treatment, but also with the seemingly healthy morphology at 5 μ M, the extracellular amino-acid profile and presynaptic function are still disturbed. Erastin, too, interferes with neuronal function while not showing any signs of damage when neurons are investigated morphologically.

As the MTT assay is very sensitive to cellular metabolism,⁵⁹ its results alone are not suited to preclude toxicity, either. The enhancement of glycolysis in sorafenib-treated cultures⁶⁰ might be responsible for the high MTT metabolism and the loss of synaptic vesicles⁴⁵ even though morphological examination clearly shows signs of toxicity for the 10 μ M concentration. The relatively low MTT metabolism rate in erastin-treated cells on the other hand might not be a sign of a weak viability but rather is the consequence of erastin's binding to mitochondrial membrane proteins (mPTP and VDAC-1²⁹).

With that, the strong changes in cell metabolism and the extracellular amino-acid regulation of sorafenib might be mediated by xCT-independent targets. In contrast, the

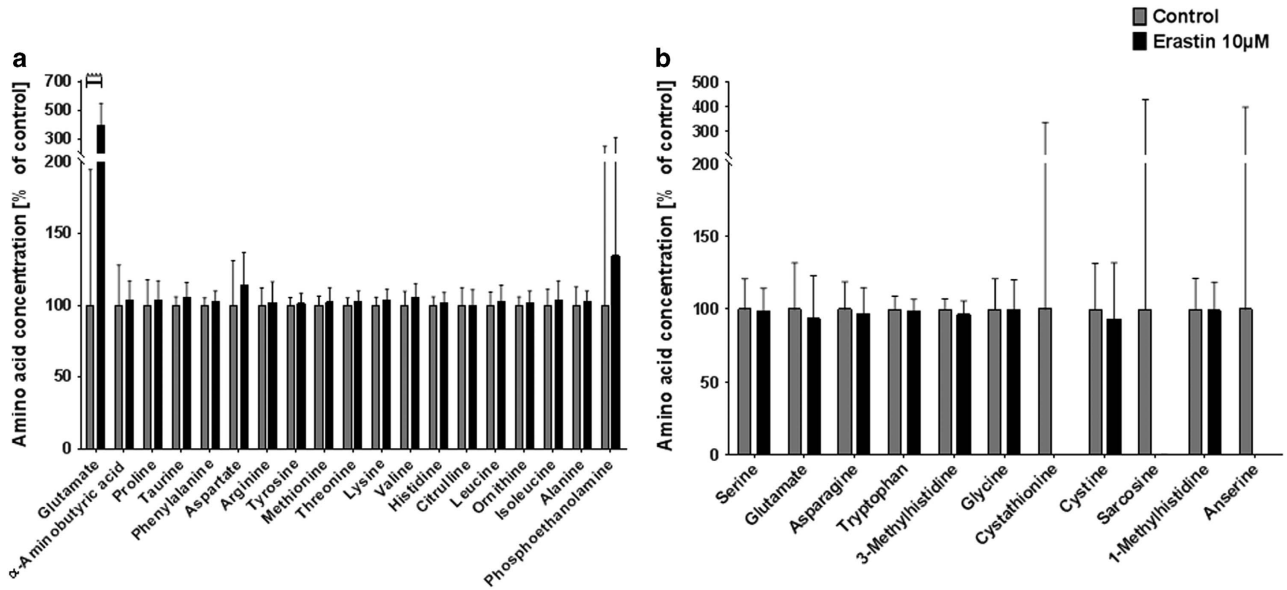


Figure 6. High-dose erastin treatment leads to critical extracellular glutamate release. Primary hippocampus cultures were incubated with 10 μM erastin (or control) for 24 h and their supernatant was collected and analyzed by high-performance liquid chromatography (HPLC). **(a)** Amino acids upregulated in response to 10 μM erastin treatment with their concentration relative to the respective controls. Asterisks indicate the level of significance in an unpaired two-sided *t*-test. The bar plot shows means with standard deviations. Number of experiments: *n* = 12 for control, *n* = 12 for 10 μM erastin. **(b)** Amino acids downregulated in response to 10 μM erastin treatment with their concentration relative to the respective controls. Asterisks indicate the level of significance in an unpaired two-sided *t*-test. The bar plot shows means with standard deviations. Number of experiments: *n* = 12 for control, *n* = 12 for 10 μM erastin. Levels of significance: ****P* < 0.001. A comprehensive table of all descriptive statistics and the analysis parameters can be found in Table 1.

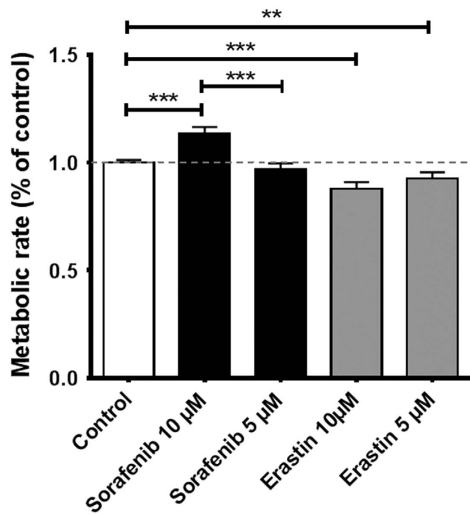


Figure 7. Metabolic rates are dose-dependently altered after sorafenib and erastin treatment. The MTT assay was performed using 3(4,5-dimethylthiazol)-2,5-diphenyltetrazolium (MTT) and detecting the rate of its metabolism to formazan in primary hippocampus cell culture. Formazan was detected measuring light absorption at 550 nm (wavelength correction 690 nm). The figure presents the pooled data of two experiments with more than six replications each, and individual controls. The data are normalized to respective controls and represent the mean with standard error of the mean. Statistical significance in two-sided *t*-test: ***P* < 0.01, ****P* < 0.001.

interference with presynaptic vesicle docking, indeed, seems to be a result of xCT inhibition, as sorafenib and erastin both interfere with the delicate regulatory system⁴⁵ mediating the recruitment of synaptic vesicles to the readily releasable pool.

Our findings of this first study on the effects of xCT inhibitors on healthy neuronal cells show that proper neuronal function cannot

be deduced solely from morphological or metabolic parameters. We applied the SOFA tool that allows an in-depth analysis of neuronal function at the synaptic level. This study also provides evidence for the hypothesis that—in addition to their desirable effect on tumor cells—sorafenib and erastin interfere with neuronal function and extracellular homeostasis, which should be taken into account when developing future chemotherapeutics on the basis of xCT inhibitors.

MATERIALS AND METHODS

If not stated otherwise, all chemicals were purchased from Sigma-Aldrich (Taufkirchen, Germany). The experiments were conducted in accordance with the local ethic guidelines of the state of Bavaria, Germany. Primary hippocampal cultures were prepared from newborn Wistar rats (Charles River, Wilmington, MA, USA) as described before.^{61,62} In short, hippocampi were removed, washed and dissociated with trypsin. After a centrifugation step they were plated on precoated glass cover slips and incubated with medium.

On the third day in culture, cells were transfected with synapto-pHluorin (spH) (PlasmidFactory, Bielefeld, Germany)⁶³ by a modified calcium phosphate method.⁶⁴ For that, the cells were incubated with transfection solution (containing 60 μl DNA, 60 μl CaCl₂, 480 μl H₂O, 2 × BBS 600 μl, 10.8 ml NBA) for 30 min, allowing calcium chloride molecules to form precipitates. Afterwards, cells were washed (HBSS) and incubated (37 °C, 5% CO₂, 95% rH) for 30 days in medium.

Prior to the experiments, the cells' medium was supplemented with 10 μM sorafenib, 5 μM sorafenib or 10 μM erastin for 24 h. These concentrations were found to efficiently target glioblastoma cell lines in previous studies.⁸ For control, cells were incubated with the respective volume of the vehicle dimethyl sulfoxide (DMSO) (Carl Roth, Karlsruhe, Germany).

Immunofluorescence staining

For an assessment of the cells' morphology, the cultures were fixated and then antibody-stained and imaged.

In detail, the cultures were washed in PBS and fixated in 4% paraformaldehyde for 15 min. The fixated cells were washed twice with PBS and then permeabilized (10 min in 1 × PBS with 0.3% Triton-X).

The samples were incubated in blocking solution containing 1 × PBS, 0.3% Triton-X and 3% fetal calf serum (Invitrogen, Taufkirchen, Germany). Primary β -tubulin III antibody (G7121, mouse monoclonal, Promega, Madison, WI, USA) was diluted in blocking solution and left on the cells for 24 h at 4 °C. The samples were then washed thrice in blocking solution and subsequently incubated for 24 h at 4 °C with the secondary antibody (Alexa Fluor 568 goat anti-mouse IgG, A-11004, Invitrogen, Taufkirchen, Germany), diluted 1:1000 in blocking solution. After washing thrice with blocking solution, the nuclei were stained with Hoechst33342, diluted 1:5000 in PBS. Images were taken with an ApoTome and the Zen Software (Zeiss, Oberkochen, Germany).

Synaptic optogenetic function analysis tool

After the sorafenib, erastin or control incubation for 24 h, the coverslips for the synaptic vesicle pool size measurement were placed in perfusion chambers, covered with 500 μ l of imaging buffer (in mM: 144 NaCl, 2.5 KCl, 10 glucose, 10 HEPES, 2.5 CaCl₂ and 2.5 MgCl₂, pH=7.5, supplemented with 80 nM concanamycin A and the corresponding treatment substance).

The fluorescence signal of the spH-transfected neuronal cell culture was recorded with a Nikon (Minato, Tokyo, Japan) TI-Eclipse inverted fluorescence microscope, equipped with a ×60, 1.2 NA water immersion objective. To stay in focus during perfusion, a Nikon Perfect Focus System was used. The fluorescent probes were excited by a Nikon Intensilight C-HGFI in a range of wavelengths 455–485 nm. The emitted light was recorded by a –90 °C water-cooled EM-CCD camera (iXonEM DU-885, Andor, Belfast, Northern Ireland), after passing an emission band-pass filter (Semrock, Rochester, NY, USA), ranging from 500 to 545 nm. The dichroic mirror had a cutoff wave length of 495 nm. A constant perfusion rate with imaging buffer (0.5 ml/min) during the recordings was ensured using a piezo-controlled perfusion system (SF-77B, Warner Instruments, Hamden, CT, USA). Constant fluid levels were maintained by using a fluid level control and a peristaltic pump (MPCU-3, Lorenz Messgerätebau, Katlenburg-Lindau, Germany).

The neurons were stimulated to release the different synaptic vesicle pools by electric field stimulation (51 mA for 1 ms, alternating polarity) delivered through two parallel platinum electrodes, spanning a distance of 10 mm. Stimulation (STG 4008, Multichannel Systems, Reutlingen, Germany) was performed in combination with a stimulus isolator (World Precision Instruments, Sarasota, FL, USA).

Recordings were exported into tagged image file (tif) format, containing 512 × 512 pixels of 16-bit monochromatic pixel values. Release of synaptic vesicles was electrically stimulated with 40 pulses at 20 Hz, evoking exocytosis of the readily releasable pool and 1200 pulses at 40 Hz, evoking exocytosis of the recycling pool.⁶⁵ The total pool was visualized by perfusion with alkaline imaging buffer containing additional ammonium chloride (50 mM). Images were acquired with an exposure time of 150 ms at a frame rate of 5 Hz.

The recorded image stacks were imported into MatLab (The Mathworks Inc., Natick, MA, USA) and further analyzed with custom-written routines. After visual inspection, measurements with no response to electrical stimuli were excluded, since a lack of excitability was seen as a lack of vitality. Synapses were then automatically detected by background-determination-based feature point detection⁶⁶ and fluorescence traces for each cell were cleared from baseline and normalized to the intensity of the total vesicle pool. The relative size of the different released vesicle pools was calculated from the stepwise increase of synaptic fluorescence upon stimulation and its linear proportionality to the relative number of released vesicles.⁵⁰

Amino-acid profiling

Metabolic assays were performed with cultures containing 10 mM glucose and 2–4 mM glutamine. To measure consumption and secretion of amino acids, cell supernatants were collected after 24 h with erastin or sorafenib and were measured by using high-performance liquid chromatography (HPLC). Amino acids were analyzed by ion-exchange chromatography and post-column ninhydrin derivatization technique using a fully automated amino-acid analyzer (Biochrom 30+, Laborservice Onken, Gröndau, Germany). For the amino-acid analysis, 100 μ l of sample was deproteinized with 100 μ l of 10% sulphosalicylic acids. Afterwards, 20 μ l of this supernatant was then loaded by the autosampler into a cation-exchange resin-filled column.

Cell metabolism analysis

To assess the treated cells' metabolic rate as a sign of cell viability, we performed a 3(4,5 dimethylthiazol)-2,5 diphenyltetrazolium (MTT) assay as described by Sehm *et al.*³¹ After 24 h, incubation with either 5 or 10 μ M sorafenib or erastin, cells were incubated with freshly made MTT solution (Roth, Karlsruhe, Germany) (5 mg/ml) for 4 h at 37 °C, 5% CO₂. We used 100 μ l isopropanol, supplemented with 0.1 N HCl for the following cell lysis. The optical density of each well was determined using the microplate reader Tecan Infinite F50 (Crailsheim, Germany) set to 550 nm (wavelength correction set to 690 nm).

Statistical analysis

If not stated otherwise, the data are given as mean with standard error of the mean and were analyzed with an unpaired two-sided *t*-test with an alpha of 0.05.

ACKNOWLEDGEMENTS

The work of MD and JKW was supported by the Else-Kröner-Fresenius Stiftung with grant 2012_A35. This study is supported by the Verein zur Förderung der Tumorforschung Mittelfranken (to NS).

AUTHOR CONTRIBUTIONS

MD performed the immunofluorescence staining experiments and SOFA analyses. He analyzed all data and took great part in writing the manuscript. EY advised MD in performing the immunofluorescence staining experiments and provided helpful guidance in writing the manuscript. DC performed the cell viability analysis and provided helpful guidance in writing the manuscript. TS advised MD and DC in performing the cell viability analysis and kindly revised the manuscript. MR performed the amino-acid profile experiments and kindly revised the manuscript. NS provided the necessary infrastructure for EY, DC and TS. He and JKW conceived the study and wrote the manuscript. JKW advised MD in conducting the SOFA analysis and she programmed the data analysis scripts. This work was performed by JKW in fulfillment of the requirements of her obtaining the degree 'Dr rer. biol. hum.' at the University of Erlangen-Nuremberg. All authors contributed to the preparation of the final manuscript and lend shape to the final version.

COMPETING INTEREST

The authors declare no conflict of interest.

REFERENCES

- Eyüpoglu IY, Buchfelder M, Savaskan NE. Surgical resection of malignant gliomas: role in optimizing patient outcome. *Nat Rev Neurol* 2013; **9**: 141–151.
- Savaskan NE, Eyüpoglu IY. xCT modulation in gliomas: relevance to energy metabolism and tumor microenvironment normalization. *Ann Anat* 2010; **192**: 309–313.
- Hambardzumyan D, Bergers G. Glioblastoma: defining tumor niches. *Trends Cancer* 2015; **1**: 252–265.
- Woehrer A, Bauchet L, Barnholtz-Sloan JS. Glioblastoma survival: has it improved? Evidence from population-based studies. *Curr Opin Neurol* 2014; **27**: 666–674.
- Stupp R, Mason WP, van den Bent MJ, Weller M, Fisher B, Taphoorn MJ *et al.* Radiotherapy plus concomitant and adjuvant temozolomide for glioblastoma. *New Engl J Med* 2005; **352**: 987–996.
- Trinh VA, Patel SP, Hwu WJ. The safety of temozolomide in the treatment of malignancies. *Expert Opin Drug Saf* 2009; **8**: 493–499.
- Takeuchi S, Wada K, Toyooka T, Shinomiya N, Shimazaki H, Nakanishi K *et al.* Increased xCT expression correlates with tumor invasion and outcome in patients with glioblastomas. *Neurosurgery* 2013; **72**: 33–41.
- Dixon SJ, Patel DN, Welsch M, Skouta R, Lee ED, Hayano M *et al.* Pharmacological inhibition of cystine-glutamate exchange induces endoplasmic reticulum stress and ferroptosis. *eLife* 2014; **3**: e02523.
- Lewerenz J, Maher P, Methner A. Regulation of xCT expression and system x (c) (-) function in neuronal cells. *Amino Acids* 2012; **42**: 171–179.
- Polewski MD, Reveron-Thornton RF, Cherryholmes GA, Marinov GK, Cassidy K, Aboody KS. Increased expression of system xc- in glioblastoma confers an altered metabolic state and temozolomide resistance. *Mol Cancer Res* 2016; **14**: 1229–1242.

- 11 Savaskan NE, Heckel A, Hahnen E, Engelhorn T, Doerfler A, Ganslandt O et al. Small interfering RNA-mediated xCT silencing in gliomas inhibits neurodegeneration and alleviates brain edema. *Nat Med* 2008; **14**: 629–632.
- 12 Dai L, Cao Y, Chen Y, Kaleeba JA, Zabaleta J, Qin Z. Genomic analysis of xCT-mediated regulatory network: identification of novel targets against AIDS-associated lymphoma. *Oncotarget* 2015; **6**: 12710–12722.
- 13 Zhai B, Hu F, Yan H, Zhao D, Jin X, Fang T et al. Bufalin reverses resistance to sorafenib by inhibiting Akt activation in hepatocellular carcinoma: the role of endoplasmic reticulum stress. *PLoS One* 2015; **10**: e0138485.
- 14 Huang Y, Dai Z, Barbacioru C, Sadee W. Cystine-glutamate transporter SLC7A11 in cancer chemosensitivity and chemoresistance. *Cancer Res* 2005; **65**: 7446–7454.
- 15 Degtrev A, Linkermann A. Generation of small molecules to interfere with regulated necrosis. *Cell Mol Life Sci* 2016; **73**: 2251–2267.
- 16 Connell LC, Harding JJ, Abou-Alfa GK. Advanced hepatocellular cancer: the current state of future research. *Curr Treat Options Oncol* 2016; **17**: 43.
- 17 Corrado A, Ferrari SM, Politti U, Mazzi V, Miccoli M, Materazzi G et al. Aggressive thyroid cancer: targeted therapy with sorafenib. *Minerva Endocrinol* 2017; **42**: 64–76.
- 18 Ferrari SM, Politti U, Spisni R, Materazzi G, Baldini E, Ulisse S et al. Sorafenib in the treatment of thyroid cancer. *Expert Rev Anticancer Ther* 2015; **15**: 863–874.
- 19 Fallahi P, Ferrari SM, Santini F, Corrado A, Materazzi G, Ulisse S et al. Sorafenib and thyroid cancer. *BioDrugs* 2013; **27**: 615–628.
- 20 Waymack JP, Moldawer LL, Lowry SF, Guzman RF, Okerberg CV, Mason AD Jr et al. Effect of prostaglandin E in multiple experimental models. IV. Effect on resistance to endotoxin and tumor necrosis factor shock. *J Surg Res* 1990; **49**: 328–332.
- 21 Shen YC, Ou DL, Hsu C, Lin KL, Chang CY, Lin CY et al. Activating oxidative phosphorylation by a pyruvate dehydrogenase kinase inhibitor overcomes sorafenib resistance of hepatocellular carcinoma. *Br J Cancer* 2013; **108**: 72–81.
- 22 Siegelin MD, Raskett CM, Gilbert CA, Ross AH, Altieri DC. Sorafenib exerts anti-glioma activity *in vitro* and *in vivo*. *Neurosci Lett* 2010; **478**: 165–170.
- 23 Zustovich F, Landi L, Lombardi G, Porta C, Galli L, Fontana A et al. Sorafenib plus daily low-dose temozolomide for relapsed glioblastoma: a phase II study. *Anticancer Res* 2013; **33**: 3487–3494.
- 24 Dolma S, Lessnick SL, Hahn WC, Stockwell BR. Identification of genotype-selective antitumor agents using synthetic lethal chemical screening in engineered human tumor cells. *Cancer Cell* 2003; **3**: 285–296.
- 25 Yagoda N, von Rechenberg M, Zaganjor E, Bauer AJ, Yang WS, Fridman DJ et al. RAS-RAF-MEK-dependent oxidative cell death involving voltage-dependent anion channels. *Nature* 2007; **447**: 864–868.
- 26 Chen L, Li X, Liu L, Yu B, Xue Y, Liu Y. Erastin sensitizes glioblastoma cells to temozolomide by restraining xCT and cystathionine-gamma-lyase function. *Oncol Rep* 2015; **33**: 1465–1474.
- 27 Kwon MY, Park E, Lee SJ, Chung SW. Heme oxygenase-1 accelerates erastin-induced ferroptotic cell death. *Oncotarget* 2015; **6**: 24393–24403.
- 28 Simamura E, Shimada H, Hatta T, Hirai K. Mitochondrial voltage-dependent anion channels (VDACs) as novel pharmacological targets for anti-cancer agents. *J Bioenerg Biomembr* 2008; **40**: 213–217.
- 29 Huo H, Zhou Z, Qin J, Liu W, Wang B, Gu Y. Erastin disrupts mitochondrial permeability transition pore (mPTP) and induces apoptotic death of colorectal cancer cells. *PLoS One* 2016; **11**: e0154605.
- 30 Tan W, Colombini M. VDAC closure increases calcium ion flux. *Biochim Biophys Acta* 2007; **1768**: 2510–2515.
- 31 Sehm T, Rauh M, Wiendieck K, Buchfelder M, Eyupoglu IY, Savaskan NE. Temozolomide toxicity operates in a xCT/SLC7a11 dependent manner and is fostered by ferroptosis. *Oncotarget* 2016; **7**: 74630–74647.
- 32 Kuo YL, Yang YK, Cheng HC, Yen CJ, Chen PS. Psychotic disorder induced by a combination of sorafenib and BAY86-9766. *Gen Hosp Psychiatry* 2014; **36**: 450.e5–450.e7.
- 33 Mulder SF, Bertens D, Desar IM, Vissers KC, Mulders PF, Punt CJ et al. Impairment of cognitive functioning during sunitinib or sorafenib treatment in cancer patients: a cross sectional study. *BMC Cancer* 2014; **14**: 219.
- 34 Magariños M, Aburto MR, Sanchez-Calderon H, Munoz-Agudo C, Rapp UR, Varela-Nieto I. RAF kinase activity regulates neuroepithelial cell proliferation and neuronal progenitor cell differentiation during early inner ear development. *PLoS One* 2010; **5**: e14435.
- 35 Liu Z, Hamamichi S, Lee BD, Yang D, Ray A, Caldwell GA et al. Inhibitors of LRRK2 kinase attenuate neurodegeneration and Parkinson-like phenotypes in *Caenorhabditis elegans* and *Drosophila* Parkinson's disease models. *Hum Mol Genet* 2011; **20**: 3933–3942.
- 36 Liu Y, Wang W, Li Y, Xiao Y, Cheng J, Jia J. The 5-lipoxygenase inhibitor zileuton confers neuroprotection against glutamate oxidative damage by inhibiting ferroptosis. *Biol Pharm Bull* 2015; **38**: 1234–1239.
- 37 Nørregaard A, Jensen SS, Kolenda J, Aaberg-Jessen C, Christensen KG, Jensen PH et al. Effects of chemotherapeutics on organotypic corticostriatal slice cultures identified by a panel of fluorescent and immunohistochemical markers. *Neurotox Res* 2012; **22**: 43–58.
- 38 Wheeler HE, Wing C, Delaney SM, Komatsu M, Dolan ME. Modeling chemotherapeutic neurotoxicity with human induced pluripotent stem cell-derived neuronal cells. *PLoS One* 2015; **10**: e0118020.
- 39 Latzer P, Schlegel U, Theiss C. Morphological changes of cortical and hippocampal neurons after treatment with VEGF and bevacizumab. *CNS Neurosci Ther* 2016; **22**: 440–450.
- 40 Satitmanwivat S, Changsangfa C, Khanuengthong A, Promthep K, Roytrakul S, Arpornsuwan T et al. The scorpion venom peptide BmK α 2 induces apoptosis in cancerous but not in normal human oral cells. *Biomed Pharmacother* 2016; **84**: 1042–1050.
- 41 Morland C, Pettersen MN, Hassel B. Hyperosmolar sodium chloride is toxic to cultured neurons and causes reduction of glucose metabolism and ATP levels, an increase in glutamate uptake, and a reduction in cytosolic calcium. *Neurotoxicology* 2016; **54**: 34–43.
- 42 Amorini AM, Lazzarino G, Di Pietro V, Signoretti S, Lazzarino G, Belli A et al. Severity of experimental traumatic brain injury modulates changes in concentrations of cerebral free amino acids. *J Cell Mol Med* 2017; **21**: 530–542.
- 43 Südhof TC. The molecular machinery of neurotransmitter release (Nobel lecture). *Angew Chem Int Ed Engl* 2014; **53**: 12696–12717.
- 44 Rizzoli SO, Betz WJ. Synaptic vesicle pools. *Nat Rev Neurosci* 2005; **6**: 57–69.
- 45 Vos M, Lauwers E, Verstreken P. Synaptic mitochondria in synaptic transmission and organization of vesicle pools in health and disease. *Front Synaptic Neurosci* 2010; **2**: 139.
- 46 Lotharius J, Brundin P. Pathogenesis of Parkinson's disease: dopamine, vesicles and alpha-synuclein. *Nat Rev Neurosci* 2002; **3**: 932–942.
- 47 Nemani VM, Lu W, Berge V, Nakamura K, Onoa B, Lee MK et al. Increased expression of alpha-synuclein reduces neurotransmitter release by inhibiting synaptic vesicle recluster after endocytosis. *Neuron* 2010; **65**: 66–79.
- 48 Cabin DE, Shimazu K, Murphy D, Cole NB, Gottschalk W, Mcllwain KL et al. Synaptic vesicle depletion correlates with attenuated synaptic responses to prolonged repetitive stimulation in mice lacking alpha-synuclein. *J Neurosci* 2002; **22**: 8797–8807.
- 49 Flechl B, Ackerl M, Sax C, Dieckmann K, Crevenna R, Gaiger A et al. Neurocognitive and sociodemographic functioning of glioblastoma long-term survivors. *J Neurooncol* 2012; **109**: 331–339.
- 50 Jung J, Loy K, Schilling EM, Rother M, Brauner JM, Huth T et al. The antidepressant fluoxetine mobilizes vesicles to the recycling pool of rat hippocampal synapses during high activity. *Mol Neurobiol* 2014; **49**: 916–930.
- 51 Kavalali ET, Jorgensen EM. Visualizing presynaptic function. *Nat Neurosci* 2014; **17**: 10–16.
- 52 Möckelmann N, Rieckmann T, Busch CJ, Becker B, Gleissner L, Hoffer K et al. Effect of sorafenib on cisplatin-based chemoradiation in head and neck cancer cells. *Oncotarget* 2016; **7**: 23542–23551.
- 53 Murthy VN, Schikorski T, Stevens CF, Zhu Y. Inactivity produces increases in neurotransmitter release and synapse size. *Neuron* 2001; **32**: 673–682.
- 54 Rosenmund C, Stevens CF. Definition of the readily releasable pool of vesicles at hippocampal synapses. *Neuron* 1996; **16**: 1197–1207.
- 55 Murphy DD, Rueter SM, Trojanowski JQ, Lee VM. Synucleins are developmentally expressed, and alpha-synuclein regulates the size of the presynaptic vesicular pool in primary hippocampal neurons. *J Neurosci* 2000; **20**: 3214–3220.
- 56 Rose CR, Ziemens D, Untiet V, Fahlke C. Molecular and cellular physiology of sodium-dependent glutamate transporters. *Brain Res Bull* 2016; e-pub ahead of print 28 December 2016; doi:10.1016/j.brainresbull.2016.12.013.
- 57 Hagberg H, Lehmann A, Sandberg M, Nystrom B, Jacobson I, Hamberger A. Ischemia-induced shift of inhibitory and excitatory amino acids from intra- to extracellular compartments. *J Cereb Blood Flow Metab* 1985; **5**: 413–419.
- 58 Bou-Hanna C, Jarry A, Lode L, Schmitz I, Schulze-Osthoff K, Kury S et al. Acute cytotoxicity of MIRA-1/NSC19630, a mutant p53-reactivating small molecule, against human normal and cancer cells via a caspase-9-dependent apoptosis. *Cancer Lett* 2015; **359**: 211–217.
- 59 Kepp O, Galluzzi L, Lipinski M, Yuan J, Kroemer G. Cell death assays for drug discovery. *Nat Rev Drug Discov* 2011; **10**: 221–237.
- 60 Tesori V, Piscaglia AC, Samengo D, Barba M, Bernardini C, Scatena R et al. The multikinase inhibitor sorafenib enhances glycolysis and synergizes with glycolysis blockade for cancer cell killing. *Sci Rep* 2015; **5**: 9149.
- 61 Röther M, Brauner JM, Ebert K, Welzel O, Jung J, Bauereiss A et al. Dynamic properties of the alkaline vesicle population at hippocampal synapses. *PLoS One* 2014; **9**: e102723.
- 62 Groemer TW, Klingauf J. Synaptic vesicles recycling spontaneously and during activity belong to the same vesicle pool. *Nat Neurosci* 2007; **10**: 145–147.

- 63 Miesenböck G, De Angelis DA, Rothman JE. Visualizing secretion and synaptic transmission with pH-sensitive green fluorescent proteins. *Nature* 1998; **394**: 192–195.
- 64 Threadgill R, Bobb K, Ghosh A. Regulation of dendritic growth and remodeling by Rho, Rac, and Cdc42. *Neuron* 1997; **19**: 625–634.
- 65 Welzel O, Henkel AW, Stroebel AM, Jung J, Tischbirek CH, Ebert K *et al*. Systematic heterogeneity of fractional vesicle pool sizes and release rates of hippocampal synapses. *Biophys J* 2011; **100**: 593–601.
- 66 Sbalzarini IF, Koumoutsakos P. Feature point tracking and trajectory analysis for video imaging in cell biology. *J Struct Biol* 2005; **151**: 182–195.



This work is licensed under a Creative Commons Attribution 4.0 International License. The images or other third party material in this article are included in the article's Creative Commons license, unless indicated otherwise in the credit line; if the material is not included under the Creative Commons license, users will need to obtain permission from the license holder to reproduce the material. To view a copy of this license, visit <http://creativecommons.org/licenses/by/4.0/>

© The Author(s) 2017